GPS Anti-Jam: A Simple Method of Single Antenna Null-Steering for Aerial Applications

Emily McMilin, David S. De Lorenzo, Thomas Lee, Per Enge: Stanford University
Dennis Akos: University of Colorado, Boulder
Stefano Caizzone, Andriy Konovaltsev: German Aerospace Center (DLR)

ABSTRACT

In this paper we introduce a backward compatible single antenna design for GPS jam mitigation on aircraft. Similar to our prior work in spoof detection [1], this anti-jam antenna requires no additional signal processing at the receiver, and it fits into the form-factor of a standard GPS antenna. There are two primary modes of operation. During the default mode, the antenna performs comparable to standard GPS antennas. During the jam mitigation mode, null steering toward the optimal azimuthal direction will generally provide greater than 10 dB of broadband signal suppression from the antenna horizon to an elevation angle about 45° below the horizon, along that azimuthal 2-D cut.

Most antenna systems that provide such broadband and wide angle jam suppression, rely on multi-antenna structures that span over a wavelengths in size, permitting the simultaneous reception of a single incident waveform at multiple phase fronts. These received signals are *phase coherent components* of the incident waveform. With the insertion of the appropriate phase shift, they can be combined to obtain constructive and destructive interference, thus steering the array's radiation beam or null in the desired direction, as can be seen schematically in Fig. 1a.

In fact, our proposed antenna is very similar. However, instead of introducing new dedicated antenna infrastructure, we reuse the (already very necessary) body of the airplane fuselage. Specifically, the conductive body of the airplane will permit the simultaneous reception of the single incident waveform at multiple phase fronts, as can be seen in Fig. 1b. However, instead of the received signals terminating at the receive ports of a multi-antenna array, the signals received by the body of the aircraft will induce surface currents on the exterior of the aircraft, some of which will eventually reach the antenna. Our proposed antenna design will permit the reception of two signals that are *phase coherent components* of a single incident waveform, when that waveform is originating from below the airplane's horizon. Similar to the concept of a large multi-antenna system, with the insertion of the appropriate phase shift, the signals can be combined to obtain destructive interference, steering a radiation null in the desired direction. Note, that this technique applies to waveforms (of any arbitrary polarization) that are originating from beneath the horizon of the aircraft, and as such, they are deemed undesirable signals that we wish to nullify. Waveforms originating from above the horizon of the aircraft are largely unaffected by this technique.

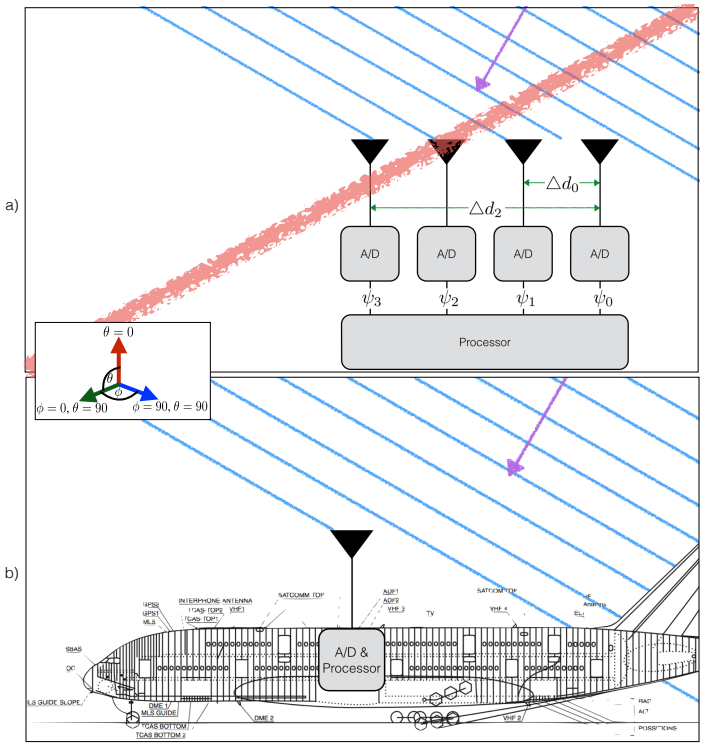

Fig. 1: Two mechanisms for obtaining the phase coherent signal components required for beam/null steering: a) the traditional method using multiple receivers with multiple antennas, and b) using a single receiver and antenna, where the antenna will receive surface currents due to placement on a large conductive ground plane. We see a) has been struck out because it will not be the focus of this paper.

SIMULATED PERFORMANCE

Fig. 2 shows the expected performance, comparing the baseline right hand circularly polarized (RHCP) radiation pattern to the anti-jam radiation pattern, when a null has been steered to the 90° azimuthal angle. We will later show other 2-D azimuthal cuts, but first focusing on this one, we see typical performance which includes almost no degradation of the signal near zenith, and greater than 10 dB of signal suppression for elevation angles ranging from just under $\pm 90^\circ$, (the horizon) to just under $\pm 135^\circ$, (45° below the horizon of the *airplane body*). The *airplane body* used for this simulation was a 800 mm diameter by 1200 mm length cylinder, that we will later see in Fig. 3c. In Fig. 2, we can see some degradation of the anti-jam performance as the elevation angle approaches nadir, where the mitigation mode actually performs worse than the baseline RHCP signal. However, we expect that as the diameter and length of the ground plane increases, to eventually reach those of practical aircraft, this undesirable back-lobe degradation will be attenuated. Later in the paper we will revisit this figure to discuss design choices, such as optimal phase shift, that was used in the generation of this simulation data.

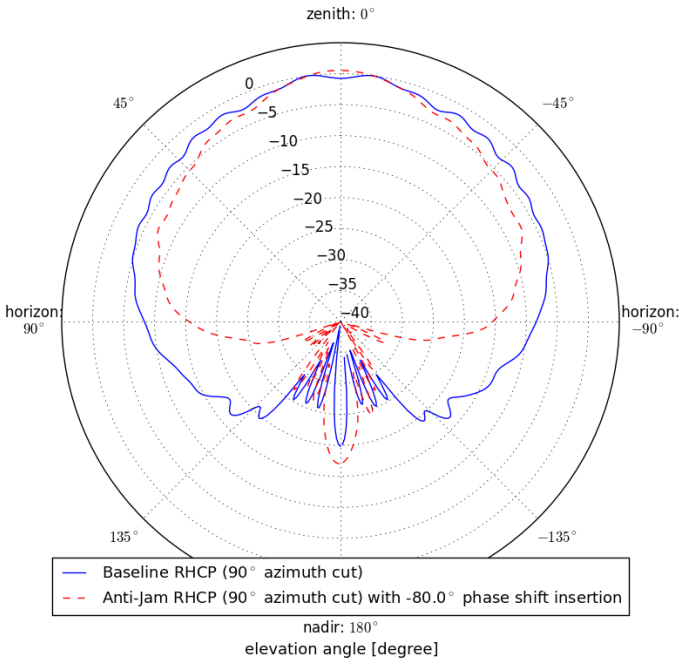

Fig. 2: Normalized RHCP far field radiation patterns, showing magnitude in dB vs elevation angle, of default mode and jam mitigation mode performance. Both patterns were derived from the same simulated data of a standard form-factor GPS antenna on a 800 mm diameter by 1200 mm length cylindrical ground plane.

PRIOR WORK

As mentioned above, most physical layer jam suppression is achieved by multiple antennas, connected to multiple radio front-ends and digitizers [2]. Although efforts to miniaturize the size of these array systems have proved successful, while still providing impressive jam suppression [3], none yet have achieved form-factor compliance with the aviation ARINC 73 antenna dimension standards of 4.7 inch by 3 inch surface area by 0.73 inch height (11.938 mm x 7.62 mm x 1.854 mm). Furthermore, most multi-antenna arrays require additional receiver hardware, calibration and computational complexity.

A single antenna design has been recently introduced [4] that can achieve robust jamming mitigation (as well as spoof detection). However this design currently suffers a constant loss of $C/N_0 \approx 6$ dB. Furthermore, this technique requires a MIMO (Multiple Input and Multiple Output) receiver that must undergo periodic self-calibration to maintain phase coherency between the two radio frequency (RF) paths that exit the single antenna. The work in [4] builds upon prior work introducing an interference suppression unit (ISU) [5], that when placed between a single GPS antenna and the receiver can provide impressive jam suppression. However, the idea published in 1998, was never further developed in later publications, perhaps due to implementation complexity. Nonetheless, the developments achieved in [4] and [5] are very promising and we draw from the polarization mismatch technique described in these papers as motivation for our work here.

BACKGROUND

Similar to what we introduce here, our own prior work also repurposed existing aspects of standard form-factor GPS antennas for new functionality, specifically spoof-detection [1]. We previously relied upon the simple fact that the GPS antenna is (by design) predominantly RHCP in the upper hemisphere of the antenna, while the lower hemisphere of the antenna (in practice), is neither predominantly RHCP nor left hand circularly polarized (LHCP). In fact, as will be discussed further in this paper, the magnitude of the RHCP and LHCP signals approach parity below the horizon of an antenna placed on a very large ground plane, such as an airplane fuselage.

In this work, we extend beyond considering only the scalar representations of these signals and instead look at the whole complex signal. Specifically, by considering the phase, as well as the magnitude, we recognize that as the elevation angle drops below the horizon, not only does the magnitude of the RHCP and LHCP signals approach parity, but also the phases of these two signals become coherent. Once phase coherency between the LHCP and RHCP signals has been established in the RF-domain, the two signals can be easily combined to produce constructive or destructive interference, by simply introducing the appropriate phase shifts just prior to the combination.

Ground plane effects

To understand the generation of the equal magnitude and phase coherent RHCP and LHCP components, we must consider the effect of the ground plane upon waveforms that are originating from below the horizon. Fig. 3 shows three different ground planes, upon which we tested an identical antenna. The antenna is a 30 mm by 30 mm square conductive patch on a 50 mm by 50 mm square substrate with a dielectric constant of 9.8 (modeled after Rogers' popular TMM 10i ceramic material). Note that this is the exact same antenna that we will revisit throughout this paper. The dimensions of the ground plane is all that varied in this experiment: a 73 mm by 73 mm square conductive ground plane, a 150 mm by 150 mm square conductive ground plane, and a 800 mm by 1200 mm cylindrical ground plane. The latter is our approximate representation of a airplane fuselage, at the upper size limit that our simulation system (running ANSYS HFSS [6]) can currently handle. In Fig. 3 we also see the 3-D CAD representations of the antenna and its respective ground plane, where the colors on the ground plane model the induced surface currents by an RHCP source.

Fig. 4 shows the *magnitude* of the RHCP and LHCP far field patterns associated with each of the three ground planes, along the 90° azimuthal cut (the circumference of the cylinder), where the RHCP signal is a solid line and the LHCP signal is a dashed line. In the case of the smallest ground plane data (green trace), we can see from the far field patterns that the RHCP and LHCP magnitudes are similar for a very small range of elevation angles around $\pm 130^\circ (40^\circ)$ below the horizon. For the medium sized ground plane (red trace), we see approximate parity between the RHCP and LHCP magnitudes at a barely wider range of elevations angles around $\pm 120^\circ (30^\circ)$ below the horizon. However, for the largest ground plane (blue trace), we can see that the RHCP and LHCP magnitudes are similar to one another over range of elevation angles spanning about $\pm 100^\circ$ to $\pm 140^\circ$ (10° to 50° below the horizon, respectively), with very good agreement from about $\pm 115^\circ$ to $\pm 140^\circ$. We expect this trend to continue, such that as the ground plane size further increases, we expect the similarities between the RHCP and LHCP magnitudes to also increase in the lower hemisphere of the antenna.

However as noted above, not only do we require the RHCP and LHCP magnitude to approach parity, we also require the RHCP and LHCP phases to become coherent across a wide range of elevation angles. Fig. 5, shows the *phase* of the RHCP and LHCP radiation patterns, associated with each of the three ground planes in Fig. 3. Again, the RHCP radiation patterns are a solid line and the LHCP radiation patterns are a dashed line, and again the traces representing each of the three ground planes retain the same color as that in Fig. 4. From Fig. 5, we can see that for the entire upper hemisphere of the antenna, the RHCP phase remains relatively flat for all three ground planes sizes. This is to be expected, as a flat phase response across elevation angle in the upper hemisphere is an important quality for a GPS antenna. Specifically focusing on the two larger ground planes (red and blue traces), we see that

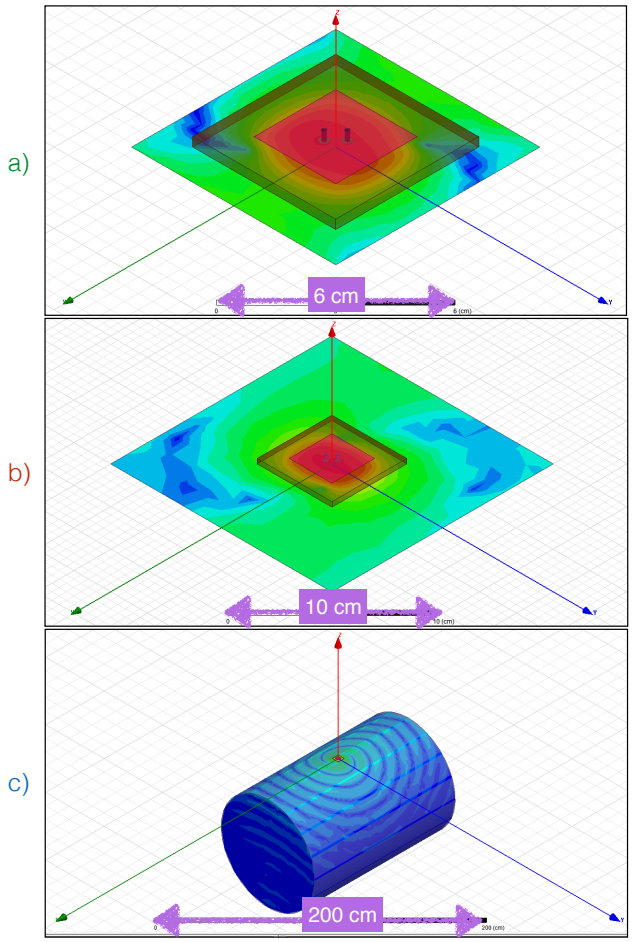

Fig. 3: Identical GPS antenna (a 30 mm by 30 mm conductive patch on a 50 mm by 50 mm substrate) simulated on three different conductive ground planes: a) 73 mm by 73 mm square, b) 150 mm by 150 mm square, and c) 800 mm by 1200 mm cylinder. CAD of antenna with ground plane showing simulated surface currents ranging from strong (red) to weak (blue).

the RHCP phase varies only by less than $\pm 5^\circ$ throughout the upper hemisphere. Also for these two larger ground planes we see reasonably good agreement between the RHCP and LHCP phases for elevation angles ranging from about $\pm 90^\circ$ (the horizon) to about $\pm 135^\circ$ (45° below the horizon). Finally, note that the wild variation of the LHCP phases near zenith is of little significance due to the low relatively value of the LHCP magnitude in this region.

We examine the phase agreement more closely in Fig. 6, which shows the *phase difference* between the RHCP and LHCP radiation patterns for the three platforms introduced above. We can see that for the largest ground plane (blue trace), the phase difference remains relatively flat, hovering about $-10^\circ \pm 5^\circ$, from an elevation angle of about $\pm 90^\circ$ (the horizon) to about $\pm 135^\circ$, (45° below the horizon). We have highlighted this region with gray bands. The 150 mm x 150 mm ground plane (red trace) does exhibits a relatively flat phase difference response over a much more narrow angular range. Finally the smallest ground-plane (green trace) shows almost no flat phase difference response over elevation

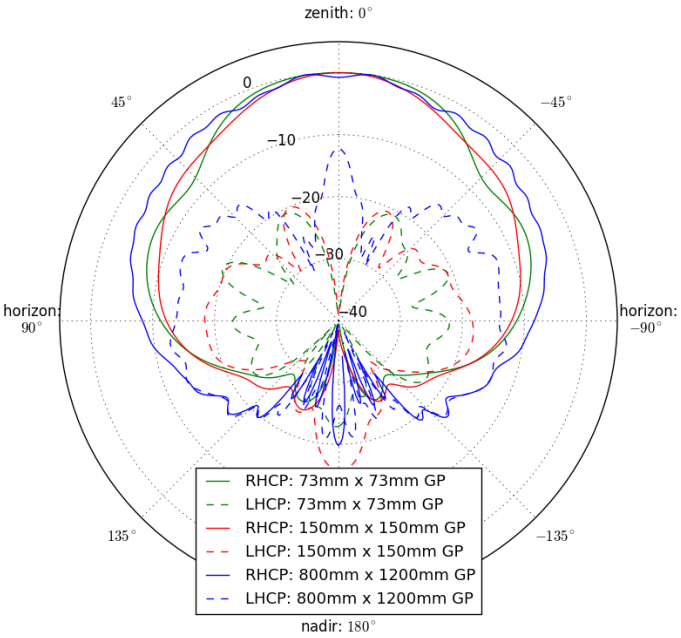

Fig. 4: Normalized RHCP and LHCP far field radiation patterns, showing magnitude in dB vs elevation angle, for the three ground planes (GP) shown in Fig. 3.

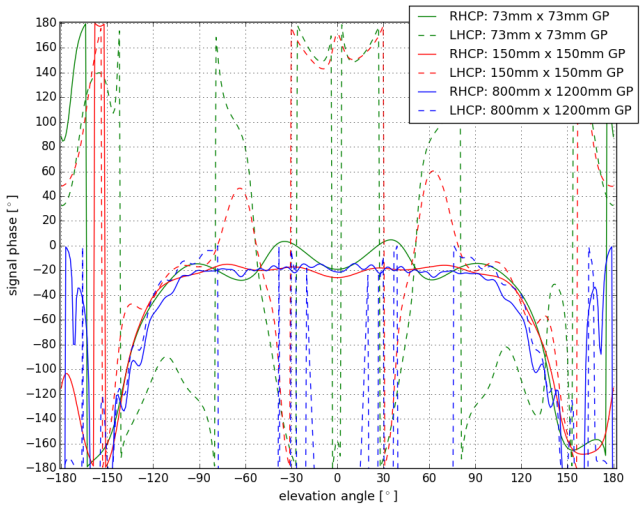

Fig. 5: Phases of the RHCP and LHCP far field radiation patterns vs elevation angle for the three ground planes (GP) shown in Fig. 3. Note the flat RHCP phase response in the upper hemisphere and the relatively good agreement between the RHCP and LHCP phases from about $\pm 90^\circ$ to about $\pm 135^\circ$.

angle.

In all three cases, we see wide variation of the difference between the RHCP and LHCP phases in Fig. 6 (and magnitudes in Fig. 3) once we reach an elevation angle beyond $\pm 135^\circ$ (within $\pm 45^\circ$ of nadir). Thus we have not obtained magnitude parity nor phase coherency over these elevation angles,

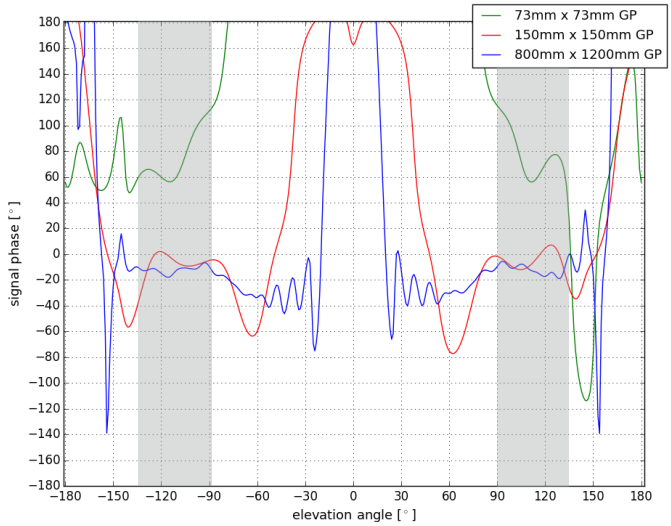

Fig. 6: Difference in phase of the RHCP and LHCP far field radiated patterns vs elevation angle for the three ground planes (GP) shown in Fig. 3. Note that the RHCP minus LHCP phase difference is relatively flat from the horizon to about $\pm 135^\circ$ for the largest GP (blue trace), as indicated by the gray bands.

and the null will not extend into this region. As will be discussed more later, we think that further increasing the ground plane beneath the antenna will help solve this problem. Extrapolating from Fig. 6 and Fig. 4, we expect that a continued increases in the size of the ground plane will show continued agreement in magnitude parity and phase coherency as elevation angles approach nadir. Finally, we also note that jam suppression at elevation angles around nadir can be considered relatively less important, when compared to elevation angles closer to the horizon, for dynamic systems. From the perspective of a moving aircraft, a stationary jamming signal will quickly transit though the elevation angles near nadir, yet dwell for a longer time as elevation angle approaches the horizon.

Before moving on, we stress the importance of achieving magnitude parity and phase coherency over the widest range of elevation angles possible. The wider the range of elevation angles for which we find good agreement between these two qualities, the broader the null we can achieve during jam mitigation. Particularly for dynamic platforms, a broad radiation pattern null is preferred over a more narrow null, which can more easily become shifted off-target or be filled in with noise.

Where does the LHCP signal come from?

But where do the LHCP signals come from in the first place? The GPS satellites produce RHCP waveforms, jammers will likely produce predominantly linearly polarized (LP) waveforms (though they may surprise us), and interference can have any arbitrary polarization. To appreciate from where the generally undesirable LHCP signals originate, we can consider a practical GPS antenna, while assuming an ideal RHCP

waveform from a satellite overhead (as a reasonable simplification). When the antenna is illuminated with an ideal RHCP waveform from directly overhead, it will do a good job of converting the waveform into an RHCP signal, with often around 80% efficiency. However, in this scenario even very good antennas will embody imperfections that convert 1 part per 100 (in the case of an axial ratio of 1.6 dB) of the RHCP waveform into an LHCP signal. As the elevation angle of the satellite drops, the antenna's conversion of RHCP waveforms into LHCP signals generally increases.

To help understand why this occurs, we can consider the decomposition of the incident RHCP waveform into two orthogonal electric field components, which are themselves orthogonal to the direction of the energy propagation. We can call these two components the x-axis field and y-axis field, distinguished by color in Fig. 7. Specifically, we see two incident waveforms as three distinct moments in time: one waveform approaching from a high elevation angle with x-axis and y-axis fields indicated in green and blue, respectively, and the other waveform approaching from the horizon with x-axis and y-axis fields indicated in purple and yellow, while the black arrows indicates the direction of propagation. At the earliest instance in Fig. 7a, we see that all field components have near equal magnitudes. However, in the later instances of Fig. 7b and 7c, we can see a large reduction in the magnitude of the y-axis component in the waveform that is approaching from the horizon. This loss in magnitude can be attributed to the high attenuation experienced by all electromagnetic waves that have a component of their electric field that is parallel to a conductive surface. Specifically, from Maxwell's Equations [8], we know that perfectly conductive surfaces will not support the parallel electric field component of an electromagnetic wave, but will propagate the perpendicular electric field component. This perpendicular field component presents itself as a vertically polarized (VP) waveform, to the GPS antenna.

The green and light blue sections of the ground planes shown in Fig. 3, provide a qualitative indication of these vertically polarized fields by highlighting the associated surface currents they induce. For signals originating from below the horizon, their journey toward the antenna atop an airplane fuselage requires some travel time along the conductive body of the airplane, thus transforming any arbitrary signal into the only type of signal that the conductive surface supports: a vertically polarized one. It is important to emphasize that regardless of original polarization of the incoming waveform, only the vertical component will survive propagation along a large conductive body. Thus any arbitrary waveform arriving from an elevation angle beneath an antenna placed on a large ground plane, should reach the antenna as a VP waveform.

However, we haven't fully developed our LHCP origin story. Initially, it may not be obvious at all as to why an incident VP waveform is synonymous with phase coherent and equal magnitude RHCP and LHCP signals. We will use a mathematical model below to show that a VP signal can be decomposed into a RHCP and a LHCP signal. In fact, any LP signal can be decomposed into a RHCP and a LHCP signal [9]. However for now, we appeal to the more well known reciprocal argument: any circularly polarized signal can be decomposed into two (spatially and temporally) orthogonal LP signals.

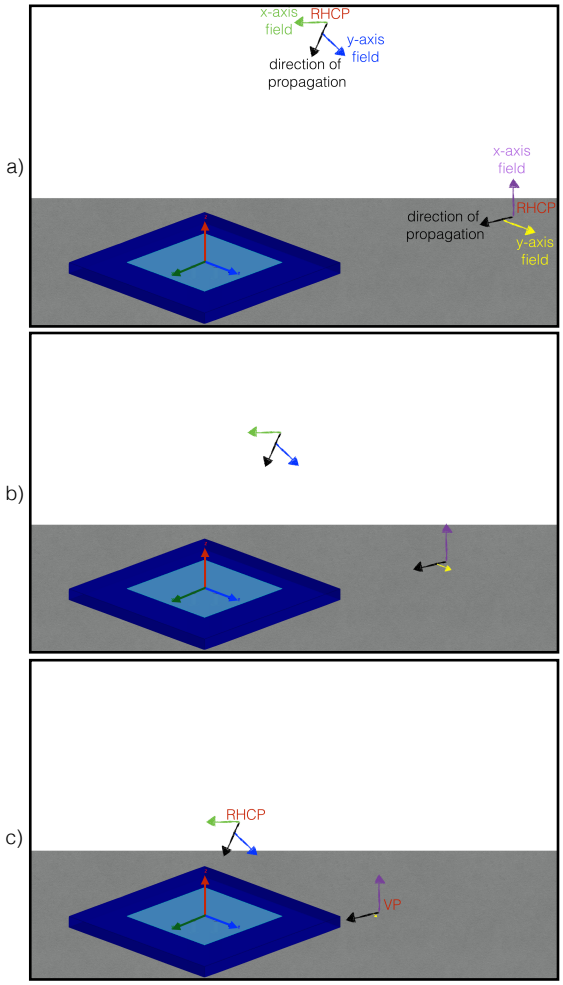

Fig. 7: Two incident waveforms at three distinct moments in time: one waveform approaching from a high elevation angle with x-axis and y-axis field components (green and blue arrows) remaining of equal magnitude, while the other waveform approaching from the horizon with x-axis and y-axis fields (purple and yellow arrows) showing a significant magnitude reduction when comparing the y-axis component at a) an earlier time instance, b) a later time instance, c) the last time instance.

When RHCP energy illuminates a GPS antenna, it often excites two orthogonal linearly polarized modes of the antenna, generating two orthogonal signals. Note that in the case of circularly polarized sources, the two resultant linearly polarized signals are orthogonal in both space (for example one is parallel to the x-axis and the other is parallel to the y-axis) and orthogonal in time (for example one signal leads the other signal by 90°).

For a standard GPS receiver, these two orthogonal signals must be processed in the RF-domain, prior to reaching the radio receiver's input. This processing transforms the two orthogonal LP signals (which are separated 90° phase shift in

time), into a single signal that the radio can consume at a single instant in time. This is generally accomplished by a *circuit element* that introduces a -90° phase shift to the leading signal, just prior to combining them together. Note that in single port antennas the function of this *circuit element* is often achieved via a distributed circuit element embodied in the antenna itself (as can be done by introducing slots or removing corners from the conductive patch), while in dual port antennas this *circuit element* is often a discrete component called a 90° hybrid coupler [7]. In both cases, only a single coaxial cable exits the antenna radome. Fig. 8 shows a standard dual port RHCP antenna, where inside antenna radome we see two orthogonal feed ports combined with a 90° hybrid coupler, with a single coaxial cable feeding the radio. This schematic is a representation of the simulation circuit we used to generate our baseline RHCP radiation patterns, that will be used for comparison to the jam-mitigation radiation patterns.

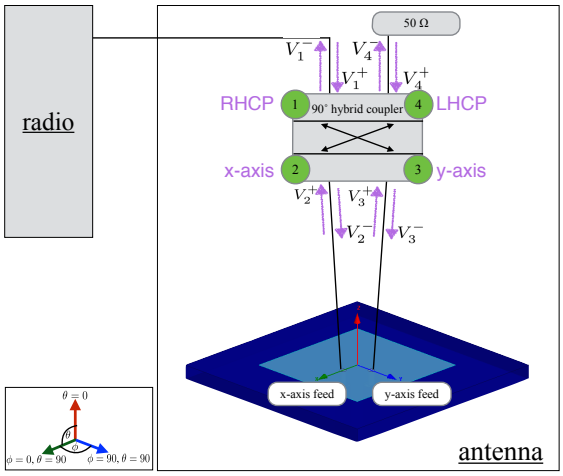

Fig. 8: Schematic of a standard dual feed RHCP antenna, where included under the radome is a 90° hybrid coupler, with its ports labeled as 1 - 4. This is a representation of the simulation circuit we used to generate our baseline RHCP radiation patterns. The annotation in purple will be explained in the next section.

MATHMATICAL MODEL

So far we have provided a qualitative description of how the geometry of the antenna and its ground plane, influences the polarization of the received signal. We will now develop a quantitative model for determining the appropriate phase shift required to steer a null toward a particular azimuthal angle. This is analogous to determining the appropriate phase shift that should be introduced into the elements of a multi-antenna array for beam/null steering. In both cases, the determination of the phase shift will permit a deterministic steering of the radiation null toward a desired direction. However, in GPS systems, the angle from which a threatening source is originating is often not known. Instead the appropriate phase shift is reached via an optimization process that can bypass any consideration of deterministic steering. However, before we can result to the more practical solution of algorithmic (or exhaustive human-driven) methods for determining the appropriate phase shift, we must understand how null steering could be achieved in the deterministic world.

Quick S-parameter primer

A compact method for explaining how this 90° hybrid coupler interacts with the incident signals arriving from the antenna, can be achieved with the use of *scattering parameters* or S-parameters. S-parameters can be used to fully characterize power flow through high frequency circuits. For example, a 4-port circuit element (S) will interact with four incoming voltage signals (V^+) to produce four outgoing voltage signals (V^-), where each voltage signal travels through its own port to its own transmission line. A total of eight voltage signals with their direction in reference to the 90° hybrid coupler (incoming or outgoing) have been annotated in Fig. 8.

$$S = \begin{bmatrix} s_{1,1} & s_{1,2} & s_{1,3} & s_{1,4} \\ s_{2,1} & s_{2,2} & s_{2,3} & s_{2,4} \\ s_{3,1} & s_{3,2} & s_{3,3} & s_{3,4} \\ s_{4,1} & s_{4,2} & s_{4,3} & s_{4,4} \end{bmatrix} \tag{1}$$

$$V^+ = \begin{bmatrix} V_1^+ & V_2^+ & V_3^+ & V_4^+ \end{bmatrix}^\top \tag{2}$$

$$V^- = \begin{bmatrix} V_1^- & V_2^- & V_3^- & V_4^- \end{bmatrix}^\top \tag{3}$$

where

$$V^- = SV^+ \tag{4}$$

In the above equations, $^\top$ signifies a transpose (but not a complex conjugate) and j represents a 90° phase shift, the subscript $_n$ indicated the port number, and finally the superscripts $^+$ and $^-$ indication a forward and reverse oriented voltage signal(respectively).

The S-parameter matrix for an ideal 90° hybrid coupler, remains static, regardless of what kind of signals couple to it, and is defined as [8]:

$$S_{90^\circ} = \frac{-1}{\sqrt{2}} \begin{bmatrix} 0 & j & 1 & 0 \\ j & 0 & 0 & 1 \\ 1 & 0 & 0 & j \\ 0 & 1 & j & 0 \end{bmatrix} \tag{5}$$

where ports 1 through 4 are labeled consistently with those shown in Fig. 8.

Circularly polarized signals

An ideal RHCP incoming signal can be represented as:

$$V_R^+ = \frac{1}{\sqrt{2}} \begin{bmatrix} 0 & 1 & j & 0 \end{bmatrix}^\top \tag{6}$$

Applying $V^+ = V_R^+$ in Equation 4, where $S = S_{90^\circ}$, we find V^-:

$$V_R^- = \begin{bmatrix} -j & 0 & 0 & 0 \end{bmatrix}^\top \tag{7}$$

Conveniently, we see that these two half-power orthogonal signals (which arrived via port 2 and port 3), have now been combined into a full power signal, traveling down port 1 to the radio, while zero energy is traveling down port 4 to the

$50\ \Omega$ load. Thus it appears an incoming RHCP signal will be transformed into an outgoing signal on port 1, only, and thus we have labeled port 1 as "RHCP" in Fig. 8. Note the value of $-j$ for the signal at port 1, simply represents a *relative* phase shift of -90° for a signal of full magnitude, and doesn't have any effect on the *absolute* value the signal. This is an ideal representation of what happens when an RHCP signal arrives from zenith.

To the contrary, we see applying an LHCP signal:

$$V_L^+ = \frac{1}{\sqrt{2}} \begin{bmatrix} 0 & j & 1 & 0 \end{bmatrix}^\top \tag{8}$$

to Equation 4, with $S = S_{90^\circ}$, we get the entire signal traveling down port 4 to the $50\ \Omega$ load, and nothing heading down port 1 to the receiver:

$$V_L^- = \begin{bmatrix} 0 & 0 & 0 & -j \end{bmatrix}^\top \tag{9}$$

Similar to the case above, it can now be seen that an incoming LHCP signal will be transformed into an outgoing signal on port 4, only, and thus we have labeled port 4 as "LHCP" in Fig. 8. The attenuation of LHCP signals in the $50\ \Omega$ load is desirable for the suppression of multi-path, during which RHCP signals will become LHCP after a single bounce off a conductive surface.

A more common scenario, even in the most ideal of circumstances, will be the inclusion of some LHCP signal in a predominantly RHCP signal. As noted above, this will occur due to any circularly polarized antenna that doesn't have a perfect axial ratio of 1. For example, a slightly more practical predominantly RHCP signal that contains 1% LHCP:

$$V_{\hat{R}}^+ = \frac{1}{\sqrt{2}} \begin{bmatrix} 0 & 0.99+0.01j & 0.01+0.99j & 0 \end{bmatrix}^\top \tag{10}$$

will combine with $S = S_{90^\circ}$, to produce signals where 99% of the signal heading to port 1 and the remaining 1% burning up in the resister at port 4.

$$V_{\hat{R}}^- = \begin{bmatrix} -0.99j & 0 & 0 & -0.01j \end{bmatrix}^\top \tag{11}$$

Vertically polarized signals

Vertically polarized signals are represented with only one phase component, instead a signal containing both a real (0°) and an imaginary (90° or j) phase component. Such relative phase shifts are only meaningful when they are relative to another component in the system, and are not an indication of the absolute phase of the signal. So, we can choose to represent the VP signals arriving at ports 2 and 3 with any relative phase we prefer and we select 0°. Furthermore, as previously established in the case of an antenna on a large aircraft body, signals originating from below the horizon will approach an antenna with a predominantly vertical polarization. Thus we will only consider ideal VP signals here, and we will consider all of these signals to be undesirable based on their presumed origin of beneath the horizon of the plane.

Adopting the coordinate system shown in Fig. 8, a VP signal arriving from an azimuthal angle of 0° will present the following incoming signal:

$$V_{V_0}^+ = \frac{1}{\sqrt{2}} \begin{bmatrix} 0 & 1 & 0 & 0 \end{bmatrix}^\top \tag{12}$$

Note that we include a minimum of a half power reduction in this signal due to the presumed attenuation of a horizontally polarized component, in the original signal, by the body of the airplane; however, as all these signals are normalized to unity, this is an arbitrary assumption.

Now combining this with Equation 4, for $S = S_{90^\circ}$, we find the incoming signal becomes equally split between the two output ports, with a relative phase shift of $-j$ at port 1:

$$V_{V_0}^- = \begin{bmatrix} -0.5j & 0 & 0 & -0.5 \end{bmatrix}^\top \tag{13}$$

Similarly, in the case of a VP signal arriving from an azimuthal angle of 90° will see the following incoming signal and respective outgoing signal, now with a relative phase shift of $-j$ at port 4:

$$V_{V_{90}}^+ = \frac{1}{\sqrt{2}} \begin{bmatrix} 0 & 0 & 1 & 0 \end{bmatrix}^\top \tag{14}$$

$$V_{V_{90}}^- = \begin{bmatrix} -0.5 & 0 & 0 & -0.5j \end{bmatrix}^\top \tag{15}$$

Two more general cases to consider are a VP signal approaching from an azimuthal angle of 45° and 135°. In this case, we would expect the signals to be split between both the x-axis feed and the y-axis feed, without any relative phase shift, producing the following incoming signal and outgoing signals:

$$V_{V_{45}}^+ = \frac{1}{\sqrt{2}} \begin{bmatrix} 0 & 0.5 & 0.5 & 0 \end{bmatrix}^\top \tag{16}$$

$$V_{V_{45}}^- = \begin{bmatrix} -0.25+-0.25j & 0 & 0 & -0.25+-0.25j \end{bmatrix}^\top \tag{17}$$

and

$$V_{V_{135}}^+ = \frac{1}{\sqrt{2}} \begin{bmatrix} 0 & -0.5 & 0.5 & 0 \end{bmatrix}^\top \tag{18}$$

$$V_{V_{135}}^- = \begin{bmatrix} -0.25+0.25j & 0 & 0 & 0.25+-0.25j \end{bmatrix}^\top \tag{19}$$

In all four cases of a VP signal arriving from azimuthal angles of 0°, 45°, 90°, and 135°, we can see that half of the signal has been sent off to the $50\ \Omega$ load at port 4. The remaining half of this undesirable signal is being sent to the receiver at port 1, exposing the receiver to potentially threatening signals. Fortunately, we know exactly what this undesirable signal at the radio looks like, as we have an identical copy of this signal (except for a relative phase shift) that is becoming heat in the $50\ \Omega$ load. Perhaps, instead of sending the signal at port 1 directly to the radio, we can first destructively combine the signal at port 1 with the signal at port 4, prior to sending the combination to the receiver?

Mitigation technique

This technique of destructively combining the two circularly polarized signals that compose the VP signal, is exactly the method we propose in this paper for suppressing undesirable incident waveforms. A high level schematic of our circuit is shown in Fig. 9. As compared to Fig. 8, two additional components have been added: a variable phase shifter and a Wilkinson power combiner. We will later introduce a more detailed circuit that switches between the standard RHCP functionality discussed above, and the anti-jam functionality that we discuss here. For now, we will assume that we are experiencing sufficiently undesirable interference from a source below the horizon of the airplane, such that we have permanently switched into the *mitigation mode* shown in Fig. 9.

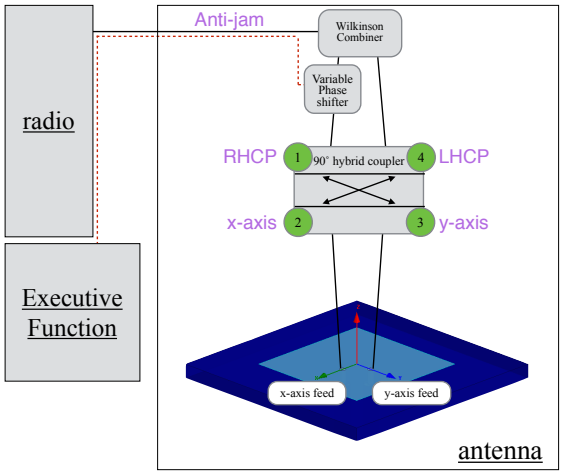

Fig. 9: Mitigation circuit, in which a variable phase shifter and a power combiner have been added to a standard dual feed RHCP antenna shown in Fig. 8. Again the 90° hybrid coupler has its ports labeled as 1 - 4.

What remains now is to find the appropriate phase shift that will steer a null toward the desired azimuthal angle. At this time we do not worry about steering toward a desired elevation angle, because we are assuming that *all* waveforms originating from the lower hemisphere will be VP, and thus be composed of two equal magnitude and phase coherent RHCP and LHCP signal components. Under this assumption, a null steered to a given azimuthal angle ϕ_c, will produce ideal jam suppression from for the angles ranging from $(\theta = \pm 90, \phi_c)$ to $(\theta = \pm 180, \phi_c)$, or the entire lower hemisphere for the 2-D cut along ϕ_c.

In reality, we know that the jam suppression is not ideal, and nor does it extend all the way from the horizon to nadir, but instead is optimal from the horizon to about $\theta = \pm 135$, as was shown in Fig. 2. Nonetheless, for the construction of a mathematical model for optimal jam suppression, we assume ideal conditions: that for waveforms originating from the lower hemisphere, ϕ is the only free variable because jam suppression at θ angles is already fixed to be an optimal value from the horizon to nadir.

We will use the notation ψ to mathematically represent the phase shift that will be introduced by the variable phase shifter in Fig. 9. Now revisiting an equation for an incoming VP waveform producing an outgoing V^- signal, for example Equation 13 for $\phi = 0°$, we can see the effect of adding the appropriate phase shift, ψ, to the outgoing port 1 signal, V_1^-. Specifically, we see that if we add an additional $\psi = 90°$, or equivalently $\psi = j$, to obtain new signal from port 1, ψV_1^-, we find a total outgoing signal of:

$$V_{\psi V_0}^- = \begin{bmatrix} \psi V_1^- & V_2^- & V_3^- & V_4^- \end{bmatrix}^\top \tag{20}$$
$$= \begin{bmatrix} (\psi)(-0.5j) & 0 & 0 & -0.5 \end{bmatrix}^\top \tag{21}$$
$$= \begin{bmatrix} (j)(-0.5j) & 0 & 0 & -0.5 \end{bmatrix}^\top \tag{22}$$
$$= \begin{bmatrix} -(0.5j^2) & 0 & 0 & -0.5 \end{bmatrix}^\top \tag{23}$$
$$= \begin{bmatrix} -(-0.5) & 0 & 0 & -0.5 \end{bmatrix}^\top \tag{24}$$
$$= \begin{bmatrix} +0.5 & 0 & 0 & -0.5 \end{bmatrix}^\top \tag{25}$$

Thus, for signals originating from an elevation angle below the horizon and an azimuth angle of 0°, after adding the $\psi = 90°$ phase shift, the signal from port 1, now $\psi V_1^- = +0.5$ is the exact opposite of the signal from port 4, still $V_4^- = -0.5$, and the two can simply be combined in the Wilkinson combiner, for perfect cancellation (in the ideal world). Thus, we have found that we can deterministically steer a null toward the azimuth angle of $\phi = 0°$ by adding a $\psi = 90°$ phase shift to port 1.

Due to symmetry, a null will *also* be steered toward the azimuth angle of $\phi = 180°$, when the $\psi = 90°$ phase shift is added at to port 1. We can see this mathematically when we look at the input / output signal combinations: V^+/V^- for $\phi = 180°$:

$$V_{V_{180}}^+ = \frac{1}{\sqrt{2}} \begin{bmatrix} 0 & -1 & 0 & 0 \end{bmatrix}^\top \tag{26}$$

and

$$V_{V_{180}}^- = \begin{bmatrix} 0.5j & 0 & 0 & 0.5 \end{bmatrix}^\top \tag{27}$$

We again find that inserting an additional phase shift of $\psi = 90°$ or j at port 1 will generate $\psi V_1^- = (j)(0.5j) = 0.5j^2 = -0.5$, a signal that is equal in magnitude but opposite in sign to the $V_4^- = +0.5$ signal at port 4. Thus, the final step of combining the two signals in the Wilkinson combiner would achieve a perfect cancelation of waveforms originating from the azimuth angle of $\phi = 180°$ and elevation angles below the horizon.

Repeating this process for azimuthal angles of $\phi = 45°$, 90° and 135° and applying symmetry, we can determine the appropriate phase shifts that should be inserted after port 1 in order to deterministically steer a null to the given azimuthal angle, as shown in Table 1.

Deterministic steering formulas

We will now formalize the above analysis into a single and simple equation that can be used to determine the appropriate phase shift required to steer a below-the-horizon-null to a

azimuthal angles (ϕ)	inserted phase shift (ψ)
0° & 180°	-270°
45° & 225°	-180°
90° & 270°	-90°
135° & 315°	0°

Table 1: Phase shift (ψ) that must be inserted to achieve deterministic steering of a null to azimuthal angle, ϕ, and to elevations angles beneath the horizon. Note that due to symmetry, a ψ has double the periodicity of ϕ.

given azimuthal angle. However, we will first revisit the more familiar scenario of the multi-antenna array shown in Fig. 1a. In this multi-antenna array, to deterministically steer a beam to an elevation angle θ, we would introduce the following phase shift, ψ_i, to the ith element of the array [9]:

$$\psi_i = 2\pi \frac{\triangle d_i}{\lambda} \sin\theta + \psi_0 \tag{28}$$

where

$$\begin{aligned} &d_0 = \text{location of reference antenna} \\ &\psi_0 = \text{initial phase offset of antenna at } d_0 \\ &\triangle d_i = d_i - d_0 \\ &\theta = \text{desired elevation angle for beam} \end{aligned} \tag{29}$$

Similarly, we can extrapolate from the work done in the prior section to develop a closed form expression for deterministic null steering in our anti-jam antenna. We precede this equation with that for multi-antenna steering, in order to highlight the similarities between these two methods. Specifically, in our anti-jam antenna, to deterministically steer a null to an azimuthal angle ϕ, we would introduce the following phase shift ψ, to port 1 of the 90° hybrid coupler:

$$\psi = 2\triangle\phi + \psi_0 \tag{30}$$

where

$$\begin{aligned} &\phi_0 = \text{orientation of antenna} \\ &\psi_0 = \text{initial phase offset of antenna at } \phi_0 \\ &\triangle\phi = \phi - \phi_0 \\ &\phi = \text{desired azimuthal angle for null} \end{aligned} \tag{31}$$

For the case of the coordinate system and orientation we used above: setting $\phi_0 = 0^\circ$ and $\psi_0 = -270^\circ$, we can see there is agreement between the outcomes of this formula and the values in Table 1.

SYSTEM DESIGN

In practice, our simulation performance rarely conformed to the ideal behavior of Equation 30. Revisiting Fig. 6, recall that the 800 mm x 1200 mm cylindrical ground plane showed a phase difference between the RHCP and LHCP signals that was relatively flat over a good portion of the elevation angles below the horizon. However, instead of the phase difference hovering about $0^\circ \pm 5^\circ$, as expected for a VP signal, we see a phase difference hovering about $10^\circ \pm 5^\circ$. Hence we see an additional, thus far unaccounted for, 10° *geometry-based* phase offset. At this time, it is unclear how the geometry of the ground-plane and the antenna affect this deviation from expectation. However we do see that it is based on geometry of the ground-plane and that is a function of ϕ. To account for this geometry-based phase offset, we must modify Equation 30 to introduce an additional ψ component that is a function of ϕ:

$$\psi = 2\triangle\phi + \psi_0 + \psi_\phi \tag{32}$$

where, in addition to Equations 31, we must add:

$$\psi_\phi = \text{geometry-based phase offset as a function of } \phi \tag{33}$$

For this paper, we determine a reasonable ψ_ϕ by using the technique discussed in the beginning of this section. Specifically, we plot the phase difference between the RHCP and LHCP signals for each azimuthal angle of interest, and then look for the deviation from the expected phase difference of about $0^\circ \pm 5^\circ$. Returning to the example we began in this section, for an azimuthal angle of 90°, Equation 30 predicts an optimal phase shift insertion value of -90°. However for the case of the 800 mm x 1200 mm cylindrical ground plane, we must include the $\psi_\phi = 10^\circ$ phase difference offset shown in Fig. 6, to reach a final optimal phase shift insertion value of -80° (as was used in Fig. 2).

We now will look qualitatively at the expected radiation patterns for both the default RHCP radiation pattern and our anti-jam pattern for the first quadrant of the sphere. Due to two bilateral symmetries, we expect the remaining 3 quadrants to resemble the one shown here. Specifically, we look at 2-D elevation cuts along constant azimuth angles of $\phi = 0^\circ,\ 30^\circ,\ 60^\circ$ in Fig. 10 (and $\phi = 90^\circ$ was already seen in Fig. 2), where we have steering a null to each given azimuth angle. We see anti-jam performance generally meeting our expectations stated earlier: greater than about 10 dB of jam suppression from the horizon to about 45° below the horizon, and generally an un-modified upper hemisphere response. As we have noted before, jam suppression for the remaining lower hemisphere elevation angles (from about 45° below the horizon to nadir) is more dependent on the form-factor of the aircraft, and we expect improved performance in this region when the proposed antenna design is tested on larger aircrafts. We also claim that the relative importance of jam suppression is reduced as elevation angles approach nadir, due to the limited dwell time that a static spoofer will remain in at this elevation angle relative to an antenna on a moving platform, when compared to elevation angles that approach the horizon.

The results seen in Fig. 10 and 2, were achieved by taking the raw data (of the x-axis and y-axis electric field components of

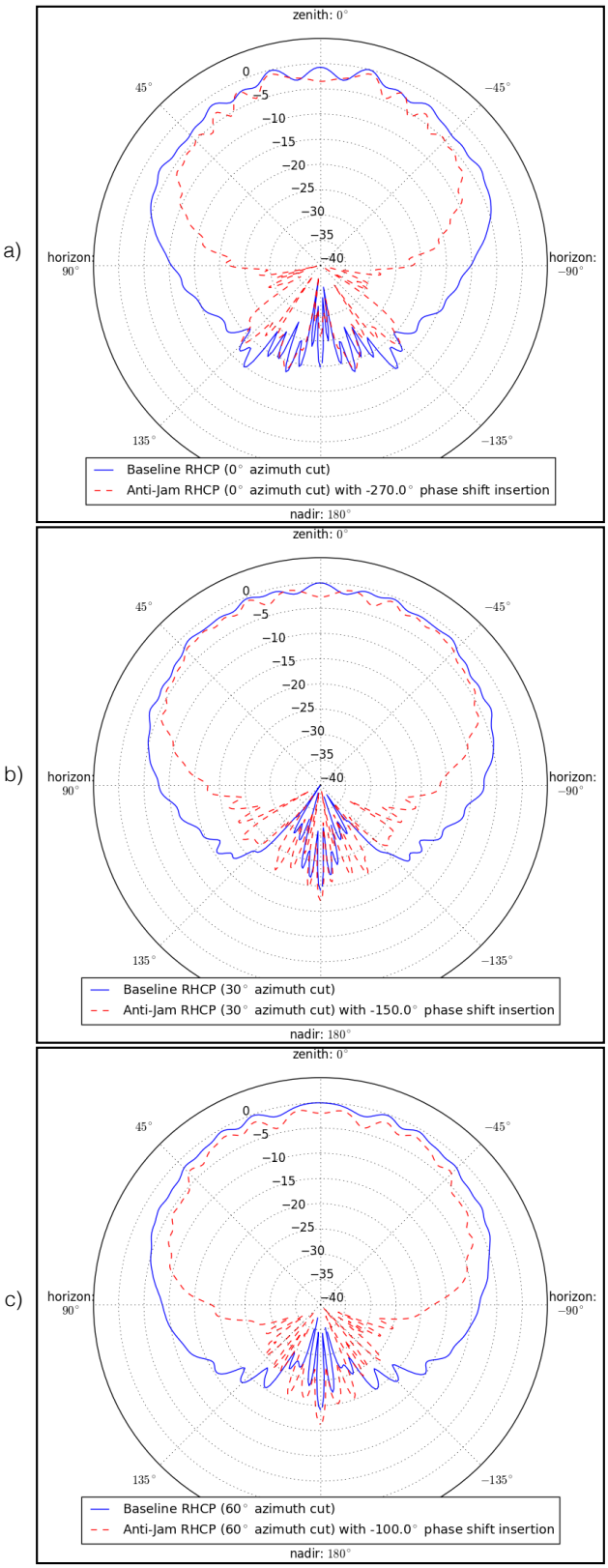

Fig. 10: Normalized RHCP far field radiation patterns, showing magnitude in dB vs elevation angle, of default mode and jam mitigation mode for the first quadrant of the simulated data, derived from the same dataset that was a first introduced in Fig. 2

the far field plot) from HFSS and post-processing in Python to simulate the 90° hybrid coupler, phase shifter and Wilkinson power combiner. Python scripts permitted systematic batch processing of large simulation files. However manual checks were performed in ANSYS Designer [6] circuit simulator to spot check the validity of the Python results.

Practical phase shifting

So far we have discussed a deterministic mapping between an azimuthal angle of interest and the proper phase shift selection. The main purpose of explaining the math behind this mapping is to motivate the relationship between the variable phase shifter and the azimuthal angle of the null steering. In this section we discuss a more practical mapping between the phase insertion applied at the variable phase shifter and our desired goal of jam suppression.

Adjustment of the phase shifter up in the antenna from a location down at the receiver, could be implemented with a simple circuit that is essentially the size of an RF barrel connector. This added circuit places the control voltage onto the inner conductor of the RF coaxial cable and could consist of a small battery, an exposed switch or dial, an RF choke, a DC blocking capacitor and a couple resisters. Note that here we have assumed that an analog phase shifter (such as the Hittite HMC934LP5E) is used at the antenna, thus requiring only a simple change in DC control voltage level for the adjustment of the variable phase shift. Note that there will be several components requiring control and supply voltages in the antenna, and thus a more sophisticated system of coupling low frequency AC voltage control signals may be required.

The exposed dial could be controlled by a human operator, effectively tuning the antenna for an optimal response. However, a more desirable implementation could involve integration with a standard GPS receiver to include a power minimization algorithm running on the receiver in the digital domain. This algorithm can adapt a DC (or low frequency modulated AC) voltage control signal, that is coupled onto the inner (or outer) conductor of the RF coaxial cable, in order to establish an optimal phase shift. We will briefly introduce one possible mechanism for this algorithm.

All receivers have an analog to digital converter (ADC) that follows the analog radio front-end, and proceeds the digital acquisition and tracking algorithms. After the ADC, the analog signal captured by the receiver is now a digital sequence n bits long, where n is the fixed number of bits used by the ADC during the conversion. For reasons soon addressed, any receiver with an ADC where $n < 1$, will also contain an automatic gain control (AGC) component [10]. ADCs have a limited dynamic range of power levels under which they can optimally convert the incoming analog signals into their digital counterparts. Thus in order to capture the largest range of incoming signals, it is desirable to place the average signal power in the middle of the ADC's dynamic range, and this is the job of the AGC.

For a quick example, we use a two bit ADC where $< 00 >$ represents the weakest signal and $< 11 >$ represents the strongest. If the AGC fails to center the average signal power in middle of this range, and instead lets it drift upward, we may find our measured samples all appear to be $< 11 >$ without variation, and thus important information has been "clipped" away and forever lost. It should also be noted that although the GPS signal power is below the thermal noise floor, the power level of the noise *signal* can undergo fluctuations and slow drifts that require an AGC to maintain optimal dynamic range at the receiver [10]. A final point worth mentioning, is that most AGCs can operate on time constants of microseconds [12], thus several orders of magnitude faster than the integration dump period of a standard GPS receiver. We therefore do not experience loss of carrier lock or other ill-effects, one might expect from a sluggish AGC.

So, we propose, as has been proposed before [11], that the AGC could be one optimal, low complexity and backward compatible mechanism for implementing the PM algorithm. Full receiver integration would only require a firmware upgrade that links the output of the AGC to the voltage signal that controls the phase shifter in the antenna, within feedback loop that will settle at the AGC's default (interference-free) baseline level.

Circuit implementation

As we mentioned previously, the results in Fig. 10 and 2, were achieved post-processing raw simulation antenna radiation pattern data with Python scripts to simulate the 90° hybrid coupler, phase shifter and Wilkinson power combiner. Despite the good agreement we see between the circuit simulation and the Python implementation, some non-idealities can get more easily brushed away when relying on Python scripts alone. For example it may not be obvious that the Wilkinson power *combiner* will sometimes (but not always) incur an insertion loss of greater than 3 dB. This is not intuitive because when the Wilkinson component is used in a reciprocal manner as a power *splitter*, the insertion loss is usually closer to 0.5 dB. If composed of ideal materials, and perfectly impedance matched, the insertion loss of the power *splitter* would be 0 dB, or perfectly loss-less. This apparent inconsistency is because even ideal 3 port network devices such as the idealized representation of a Wilkinson power combiner/splitters is loss-less when acting as a power *splitter* and *only* in certain scenarios when acting as a power *combiner*. These losses are incurred in the power *combiner* arrangement, despite our assumption of ideal materials and perfect impedance matching [8].

A quick example can serve to illustrate: a 3 dBm signal power at the combined *output* port of such a combiner can be derived in one of many ways, including the two following scenarios: a) phase coherent 0 dBm signals at both *input* ports, or b) a non-phase coherent combo of $-\infty$ dBm at one *input* port and 6 dBm at the other *input* port. In scenario (a) we have a loss-less combination of the two signals, but in scenario (b) we have lost half our signal power. Where does this signal power go? The answer to this question is that there is in fact a resister that is hidden inside the Wilkinson power divider (between the two *input* ports). When the signals presented at the two *input* are identical (as is the case in scenario (a)), there is no current flowing across this internal resister because the voltage levels on either side of the resister are identical [13]. However, in scenario (b) when one input signal is approaching $-\infty$ dBm, we will find that half the power of the other signal will be dropped across the internal resister. For the predominantly VP signals originating from the lower hemisphere, we have scenario (a) in which the two *input* signals (namely the RHCP and the LCHP signals) will be combined in an almost loss-less fashion, whereas for signals originating at zenith we have scenario (b), in which we lose about 3 dB from this predominately RHCP signal that is arriving at one *input* (while the 2nd *input* port is around -20 dBm. Thus we have the scenario where 3 dB of loss could be incurred at zenith, but not along the horizon.

Increasing the noise figure by about 3 dB is clearly undesirable. Additionally, we haven't yet taken into account the approximate 3.5 dB loss of the phase shifter and the 1 dB loss of the switches (that we will introduce shortly). To address this problem, we propose placing LNAs immediately after after the two feeds for the antenna, specifically at the x-axis and y-axis feeds points as shown in Fig. 11. This solution is expected to reduce additional noise figure increases to about 0.5dB, which has been included in the Python simulations. It is important that these two LNAs have matched phase responses; for example LNAs from the same manufacturer and even from the same silicon batch. However, as we will address shortly, the adaptive tuning of the phase shifter in the RHCP signal path can help correct for some of the drifting that may occur.

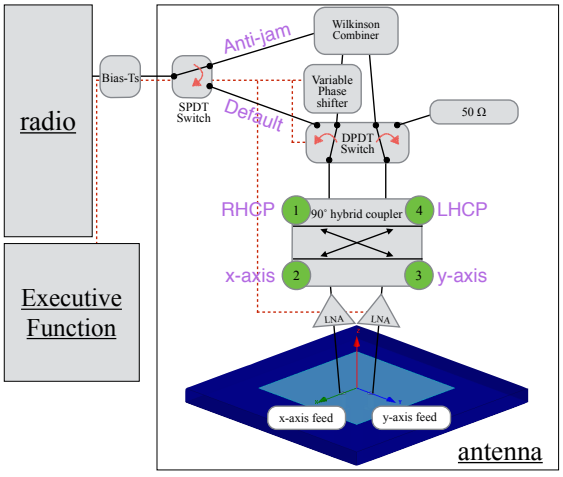

Fig. 11: Full mitigation mode and default mode circuits, having now added the LNAs and switches under the radome, with again the 90° hybrid coupler ports labeled as 1 - 4.

Fig. 11 also shows the mechanism by which an algorithm or an operator can select the jam mitigation mode or the default RHCP mode. The representation in the figure shows the ac-

tive mode as the jam mitigation mode the switches. We will complete final component selection for prototyping in future work. However at the present time, we have identified likely candidates for these components as shown in Table 2.

component	manufacturer	part number
DPDT switch	Skyworks	SKY13381-374LF
SPDT switch	Skyworks	SKY13370-374LF
90° hybrid coupler	Anaren	C1517J5003AHF
Phase shifter	Hittite	HMC934LP5E
Wilkinson combiner	Anaren	PD0922J5050S2HF
LNA	Avago	MGA-634P8

Table 2: Components that are good candidates for implementation.

Summation mode

A question remains in regard to what happens at all the other azimuthal angles when a null is being steered toward one particular azimuth angle? We know that the phase shift insertion value of ψ has twice the periodicity of the azimuthal angle ϕ, so, we would expect that steering a null toward an azimuth angle ϕ_c will also produce a null at azimuth angle $\phi_c + 180°$. Thus, appealing to symmetry, we can expect optimal jam suppression responses at azimuth angles separated by $180°$. Also appealing to symmetry, we can expect worst case jam suppression responses at azimuth angles separated by $\phi_c \pm 90°$, when a null has been steered to ϕ_c.

To first get a quantitive sense of this worst case jam suppression, we consider mathematically what would happen when we apply the deterministic phase shift required to steer a null to an azimuth angle of $\phi_c = 90°$, while examining the signal response for a waveform arriving from an azimuth angle of $\phi_c - 90° = 0°$. To deterministically steer a null toward $\phi = 90°$, we would use a phase shift of $\psi = -90°$, so we apply this $\psi = -90°$ to the equation for a lower hemisphere VP waveform arriving from azimuth angle of $\phi = 0°$ (Equation 13):

$$V^-_{\psi V_0} = \begin{bmatrix} (\psi)(0.5j) & 0 & 0 & 0.5 \end{bmatrix}^\top \quad (34)$$

$$= \begin{bmatrix} (-j)(0.5j) & 0 & 0 & 0.5 \end{bmatrix}^\top \quad (35)$$

$$= \begin{bmatrix} -(0.5j^2) & 0 & 0 & 0.5 \end{bmatrix}^\top \quad (36)$$

$$= \begin{bmatrix} -(-0.5) & 0 & 0 & 0.5 \end{bmatrix}^\top \quad (37)$$

$$= \begin{bmatrix} 0.5 & 0 & 0 & 0.5 \end{bmatrix}^\top \quad (38)$$

We again find that inserting an additional phase shift of $\psi = 90°$ or j at port 1 will generate $\psi V_1^- = (j)(0.5j) = 0.5j^2 = -0.5$, a signal that is equal in magnitude but opposite in sign to the $V_4^- = +0.5$ signal at port 4. Thus, the final step of combining the two signals in the Wilkinson combiner would achieve a perfect cancelation of waveforms originating from the azimuth angle of $\phi = 180°$ and elevation angles below the horizon.

Rather than producing signals at port 1 and 4 that are opposite of one another, we have produced identical signals: $\psi V_1^- = 0.5$ and $V_4^- = 0.5$. Thus, the combined signal will double in magnitude at the Wilkinson combiner. So, we see that at azimuthal angles orthogonal to the direction of null steering, we will get summation of the RHCP and LHCP component signals, rather than cancellation. At azimuthal angles in between the two theoretical extremes of perfect cancellation and perfect summation, we expect to see a smooth transition.

The summation signal is particularly concerning, because as was the case for the cancellation occurring primarily in the lower hemisphere of the antenna, so will this summation occur primarily in the lower hemisphere of the antenna. Thus we could be exposing the antenna to even more threatening signals from below. This can be seen in qualitatively in Fig. 12, where in simulation we looked at the radiation pattern for the $0°$ azimuthal cut, after steering a null toward a $90°$ azimuthal angle.

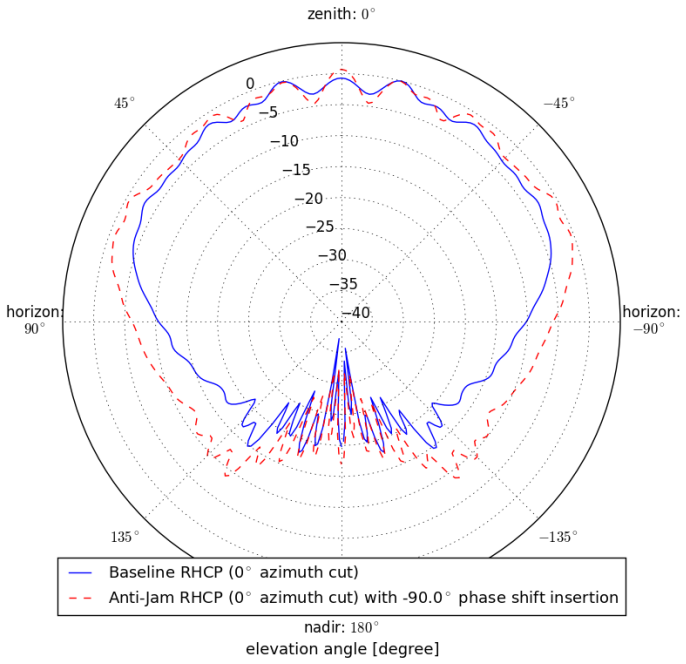

Fig. 12: Normalized RHCP far field radiation patterns, showing magnitude in dB vs elevation angle, of default mode and jam mitigation mode for the $0°$ azimuthal cut, when a null has been steered to an orthogonal $90°$ azimuthal angle.

Larger ground planes

Examination of Fig. 12, and further consideration of our expectations as the ground plane size scales up, present a less dire outlook than that of the prior paragraph. We are more accustomed to seeing the typical GPS antenna patterns with relatively small ground planes, and in free-space simulations or measurement (for example those shown in Fig. 3a and 3b)

where the back lobe is dominated by the LHCP radiation pattern. However, for larger ground planes, we no longer see a back lobe domination of LHCP, and we instead see are more likely to see the LHCP radiation pattern creeping up into the lower elevations of the *upper* hemisphere of the antenna. In addition to our simulated data in Fig. 3c, we see both measured and simulated data from relatively larger aircraft ground planes in Figs. 13 [15] and 14 [14], respectively. All three of these figures show that in the lower hemisphere, the magnitude of RHCP and LHCP signals approach parity, and that the LHCP signal has a more significant presence in the upper hemisphere, particularly at the lower elevation angles. All this helps us conclude that although the summation behavior will undesirably increase sensitivity in the lower hemisphere, it may also have a desired effect of increasing the sensitivity of the antenna in the upper hemisphere, particularly at low angles of elevation. This presents another potential feature of this antenna: when jamming is not present and increased sensitivity is desired at low angles of elevation near the horizon, for example during landing, take-off or sharp banked curves, the antenna can be switched to this *summation mode*. However we also face the presently unresolvable problem that when jamming sources are located at widely separated angles along the horizon of the plane (particularly when two jammers are at right angles to one another), the *mitigation mode* of the antenna may cause more harm than good.

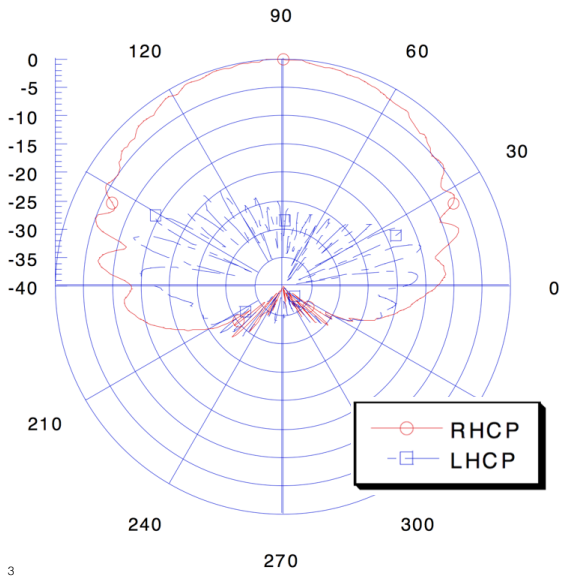

Fig. 13: Measured RHCP and LHCP patterns on the fuselage of a scaled-down F-16 jet [14].

We also use Fig. 13 and 14 to help justify our claims that jam suppression in the back lobe will improve as the ground plane increases in size. Both of these results show very good agreement between the magnitudes of the RHCP and LHCP signals at elevation angles within 45° of nadir, which is where we saw divergence of the RHCP and LHCP signals from our simulated data. Unfortunately, we have only magnitude information and not phase information for the two plots shown in Fig. 13 and 14. But based on our evaluation in this paper, we expect phase coherency between the RHCP and LHCP signals as well.

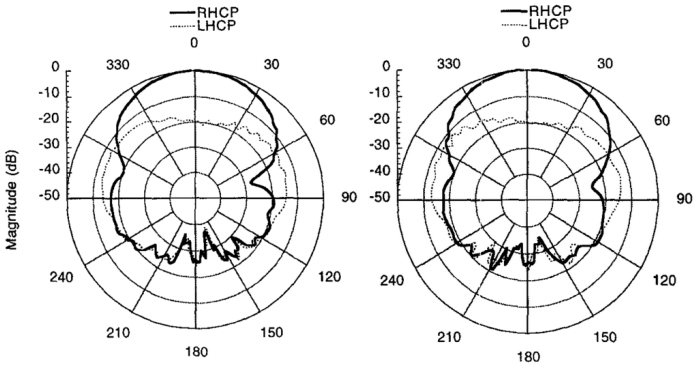

Fig. 14: Simulated RHCP and LHCP patterns on the fuselage of a airplane-like object [15].

CONCLUSIONS AND FUTURE WORK

In this paper we have introduced a single antenna design for GPS jam mitigation in aircraft applications. We have described a deterministic method of null-steering the antenna and discussed more practical methods for nulling interference. We have shown simulation results that achieve greater than 10 dB of broadband signal suppression from near the antenna horizon to about 45° below the horizon, when the antenna has been null steered toward a given azimuthal angle. The data provided was simulated on a 800 mm diameter by 1200 mm length cylindrical ground plane, and we have provided evidence for our expectation of superior performance on larger, aircraft-sized ground plane structures.

Similar to our prior work, we have exploited aspects of existing antennas and associated infrastructure to introduce new functionality. In this case we introduced jam mitigation and our prior work developed spoof-detection. Future work will be directed toward the integration of these two features into a standard form-factor GPS antenna that has been designed for aviation applications. We also intend to prototype and provide real measurement data in future work.

ACKNOWLEDGMENTS

The research conducted for this paper took place at the Stanford University Global Positioning System Research Laboratory with funding from the WAAS program office under FAA Cooperative Agreement 12-G-003.

REFERENCES

[1] E. McMilin, D. S. De Lorenzo, T. Walter, T. H. Lee, P. Enge, “Single Antenna GPS Spoof Detection that is Simple, Static, Instantaneous and Backward Compatible

for Aerial Applications," Proceedings of the 27th International Technical Meeting of The Satellite Division of the Institute of Navigation (ION GNSS+ 2014), Tampa, FL, September 2014, pp. 2233-2242.

[2] Y.-H. Chen, S. Lo, D. Akos, D. S. De Lorenzo, P. Enge, "Validation of a Controlled Reception Pattern Antenna (CRPA) Receiver Built From Inexpensive General-purpose Elements During Several Live-jamming Test Campaigns," *Proceedings of the 2013 International Technical Meeting of The Institute of Navigation*, San Diego, California, January 2013, pp. 154-163.

[3] A. Konovaltsev, S. Caizzone, M. Cuntz, M. Meurer, "Autonomous Spoofing Detection and Mitigation with a Miniaturized Adaptive Antenna Array," *Proceedings of the 27th International Technical Meeting of The Satellite Division of the Institute of Navigation*, Tampa, FL, September 2014, pp. 2853-2861

[4] T. Kraus, F. Ribbehege and B. Eissfeller, "Use of the Signal Polarization for Anti-jamming and Anti-spoofing with a Single Antenna," *Proceedings of the 27th International Technical Meeting of The Satellite Division of the Institute of Navigation*, Tampa, FL, September 2014, pp. 3495-3501.

[5] M. W. Rosen, M. S. Braasch, "Low-Cost GPS Interference Mitigation Using Single Aperture Cancellation Techniques," *Proceedings of the 1998 National Technical Meeting of The Institute of Navigation*, Long Beach, CA, January 1998, pp. 47-58.

[6] ANSYS, "HFSS", `http://www.ansys.com/Products/Simulation+Technology/Electronics/Signal+Integrity/ANSYS+HFSS`

[7] B. Rama Rao, W. Kunysz, R. L. Fante and K. F. McDonald, *GPS/GNSS Antennas*, Artech House, 2013

[8] D. M. Pozar, *Microwave Engineering, 4th Ed.*, John Wiley & Sons, 2012, pp. 343.

[9] W. L. Stutzman, *Polarization in Electromagnetic Systems*, Artech House, 1993, pp. 24.

[10] D. Akos, "Who's Afraid of the Spoofer? GPS/GNSS Spoofing Detection via Automatic Gain Control (AGC)", *Navigation*, 59: 281-290. doi: 10.1002/navi.19.

[11] F. Bastide, D. Akos, C. Macabiau, B. Roturier "Automatic Gain Control (AGC) as an Interference Assessment Tool", Proceedings of the 16th International Technical Meeting of the Satellite Division of The Institute of Navigation (ION GPS/GNSS 2003), Portland, OR, September 2003, pp. 2042-2053.

[12] Maxim Integrated, MAX2769, "Universal GPS Receiver", `http://datasheets.maximintegrated.com/en/ds/MAX2769.pdf`

[13] T. H. Lee, "Planar Microwave Engineering", Cambridge University Press, 2004.

[14] B. R. Rao, J. H. Williams, "Measurements on a GPS Adaptive Antenna Array Mounted on a 1/8-Scale F-16 Aircraft," *Proceedings of the 11th International Technical Meeting of the Satellite Division of The Institute of Navigation (ION GPS 1998)*, Nashville, TN, September 1998, pp. 241-250.

[15] B. R. Rao, M. N. Solomon, M. D. Rhines, L. J. Teig, R. J. Davis, E. N. Rosario, "Research on GPS Antennas at MITRE" *The MITRE Corporation*.